First high-resolution analysis of the $4\nu1+\nu3$ band of nitrogen dioxide near 1.5 μm

A. Perrin, Samir Kassi, Alain Campargue

First high-resolution analysis of the $4\nu_1+\nu_3$ band of nitrogen dioxide near 1.5 µm

Agnès Perrin [a§], Samir Kassi [b] and Alain Campargue [b]

[a] *Laboratoire Inter-Universitaire des Systèmes Atmosphériques (LISA), UMR 7583 CNRS et Universités Paris-Est Créteil et Paris 7 Denis Diderot, 61 Avenue du Général de Gaulle, 94010 Créteil Cedex, France*
[b] *Laboratoire de Spectrométrie Physique (associated with CNRS, UMR 5588), Université Joseph Fourier de Grenoble, B.P. 87, 38402 Saint-Martin-d'Hères Cedex, France.*

Nb of Figures: 5

Nb of Tables: 5

§ Corresponding author: A. Perrin, Laboratoire Inter-Universitaire des Systèmes Atmosphériques, LISA-UMR 7583 CNRS / Universités Paris 12 et Paris 7, 61 Avenue du Général de Gaulle, 94010 Créteil Cedex, France, Tel. 33(0)145176557, Fax. 33(0)145171564 E-mail: Agnes.Perrin@lisa.univ-paris12.fr

Abstract

The high-resolution absorption spectrum of the $4\nu_1+\nu_3$ band of the $^{14}N^{16}O_2$ molecule was recorded by CW-Cavity Ring Down Spectroscopy between 6575 and 6700 cm^{-1}. The assignments involve energy levels of the (4,0,1) vibrational state with rotational quantum numbers up to K_a = 8 and N = 48. A large majority of the spin-rotation energy levels were reproduced within their experimental uncertainty using a theoretical model which takes explicitly into account the Coriolis interactions between the spin rotational levels of the (4,0,1) vibrational state and those of the (4,2,0) and of (0,9,0) dark states, the anharmonic interactions between the (4,2,0) and (0,9,0) states together with the electron spin-rotation resonances within the (4,0,1), (4,2,0) and (0,9,0) states. Precise vibrational energies, rotational, spin-rotational, and coupling constants were determined for the {(4,2,0), (0,9,0), (4,0,1)} triad of interacting states. Using these parameters and the value of the transition dipole moment operator determined from a fit of a selection of experimental line intensities, the synthetic spectrum of the $4\nu_1+\nu_3$ band was generated and is provided as Supplementary Material.

Keywords: $^{14}N^{16}O_2$; Nitrogen dioxide; High-resolution infrared spectrum; Electron spin-rotation resonance; Coriolis resonance; Anharmonic interaction; Line position; Line intensity**,** Cavity Ring Down Spectroscopy, CRDS

1. Introduction

Nitrogen dioxide ($^{14}N^{16}O_2$) is an important atmospheric trace species involved in the photochemistry of the stratosphere and in the pollution of the troposphere. Accurate measurements of NO_2 concentration in the atmosphere are now commonly performed in the 6.2 and 3.4 μm regions which correspond to the ν_3 and $\nu_1 + \nu_3$ bands, respectively, by means of infrared remote sensing methods [1, 2]. For this reason numerous detailed spectroscopic studies of the $^{14}N^{16}O_2$ absorption bands were performed from the microwave up to the 1.7 μm region [3-11]. The results of these studies lead to lists of NO_2 line positions and intensities [12] which are now implemented in spectroscopic databases such as HITRAN [13] and GEISA [14].

$^{14}N^{16}O_2$ is an asymmetric rotor exhibiting in the infrared region a spectrum with a doublet structure due to the electron spin-rotation interaction, and a hyperfine structure in microwave and far infrared spectral regions. Also depending on the spectral range of interest, one has to consider rovibrational interactions in order to account for the measured line positions and intensities. Indeed strong C-type Coriolis resonances are coupling the spin-rotational levels of the (v_1, v_2, v_3) and (v_1, $v_2\pm2$, $v_3\mp1$) vibrational states [6, 8, 9, 10, 11, 15]. In addition, for the first triad of interacting states {(1,0,0),(0,2,0),(0,0,1)}, a weaker C-type Coriolis resonance connects the (1,0,0) and (0,0,1) energy levels [6].

It is also important to understand the complex absorption behavior of the NO_2 species at high energies. Using the laser induced dispersed fluorescence (LIDFS) technique, the complete set of the 191 lowest vibrational levels of the X^2A_1 ground electronic state, up to 10000 cm^{-1} was measured [16]. However, at wavelengths smaller than 2.5 μm only some NO_2 infrared bands were the subject of detailed rotational analysis, like the $2\nu_1+\nu_3$, $3\nu_3$ [11], $3\nu_1+\nu_3$ [17] and $\nu_1+3\nu_3$ [15] bands located at 4179.938, 4754.209, 5437.54 and 5984.705 cm^{-1}, respectively. Indeed in this frequency range, the absorption bands become extremely weak, except for

series of A-type bands corresponding to (v_1,v_2,v_3)-(0,0,0) vibrational transitions with, v_3=odd for symmetry reasons, high vibrational excitation of the stretching modes (v_1+v_3= high), and no excitation of the bending mode (v_2=0). One has to underline that during the investigation of the ν_1+3ν_3 band [15], additional high order vibration-rotation interactions involving vibrational states differing by a large number of vibrational quanta were identified in addition to the resonances classically observed in the infrared region. It is interesting to search for such high order resonances by investigating NO_2 bands at higher frequency.

The present work is devoted to the analysis of the $4\nu_1 + \nu_3$ band near 6677 cm^{-1}. This band is the highest combination band of nitrogen dioxide in the X^2A_1 ground state reported so far at high-resolution. The spectrum was recorded in Grenoble by CW-Cavity Ring Down Spectroscopy (CW-CRDS). The analysis was performed by using a Hamiltonian matrix which explicitly accounts for the electron spin-rotation resonances, Coriolis-type resonances and anharmonic interactions.

2. Experimental details

The high-sensitivity absorption spectrum of nitrogen dioxide was recorded in the 6575-6700 cm^{-1} region. The fibered distributed feedback (DFB) laser CW-CRDS spectrometer used for these recordings has been described in Refs.[18-20]. Each DFB laser diode has a typical tuning range of about 35 cm^{-1} by temperature tuning from -5°C to 60°C. Five DFB laser diodes were sufficient to cover the 6575-6700 cm^{-1} region of interest. The stainless steel ringdown cell (l= 2 m, Φ= 10 mm) is fitted by a pair of super-mirrors. The reflectivity of the used mirrors corresponds to ring down times of about τ~ 70 μs. About one hundred ringdown events were averaged for each spectral data point, and the complete temperature scan of one DFB laser required about 70 minutes. Our achieved noise equivalent absorption is typically $\alpha_{min} \sim 3\times10^{-10}$ cm^{-1} over the whole spectrum but in the present case, the absence of spectral

sections free of absorption lines made its estimation difficult. The pressure of the nitrogen dioxide sample (Sigma Aldrich, 99% purity) was fixed to 10.0 Torr measured by a capacitance gauge, and the cell temperature was 297 K. In these conditions, the nitrogen dioxide sample consists in a mixture of NO_2 and N_2O_4. The monomer partial pressure was determined using the equation:

$$P(NO_2)^2 = K_p . P(N_2O_4) \quad (1)$$

where K_P is the equilibrium constant whose value is about 81 Torr at 297 K [21]. The resulting NO_2 partial pressure is $P(NO_2)$= 9.0 (1) Torr .

Each 35 cm^{-1} wide spectrum recorded with one DFB laser was calibrated independently on the basis of the wavelength values provided by a Michelson-type wavemeter (Burleigh WA-1650, 60 MHz resolution and 100 MHz accuracy). The calibration was further refined by stretching the whole spectrum in order to match accurate positions of reference lines of H_2O present as an impurity in the sample. The H_2O line positions as provided in the HITRAN database [13] were used for calibration. The typical uncertainty on the line positions is estimated to be 1×10^{-3} cm^{-1}. An overview of the spectrum between 6620 and 6700 cm^{-1} is included in Fig. 1.

3. Analysis

3.1. Assignment

Nitrogen dioxide is an asymmetric rotor which is rather close to the prolate symmetric top limit, due to the value of its rotational constants (A~8.0023, B~0.4337, C~0.4104 cm^{-1} in the ground vibrational state [5]). According to symmetry properties, the $4\nu_1+\nu_3$ band is an A-type band with only ΔK_a = even transitions. However since NO_2 is a near prolate symmetric top, only $K_a = 0$ transitions are observable.

In principle $^{14}N^{16}O_2$ exhibits a spectrum with doublet structure due to the electron spin–rotation interaction. However, for A-type bands the observed doublets, which correspond to the difference of the spin–rotation splittings in the upper and lower states of each transition, are usually weak. The rather large Doppler linewidths in the studied region (FWHM~0.006 cm^{-1} at 1.5 μm) made these doublets difficult to resolve in our spectrum. These observations were possible for low K_a values (K_a=0,1,2) or for small N values as illustrated in Figs. 2 and 3.

The analysis of the $4\nu_1+\nu_3$ band was not easy. The Q branch is rather congested as usual for A-type bands (see Fig. 4). The R branch is also very crowded due to a turn around near 6691 cm^{-1} (see Fig. 5). For this reason, it is not always possible to rely on combination differences relations for the identification of weaker lines in the P branch. Indeed lines present in the low frequency range of the $4\nu_1+\nu_3$ band may belong to hot bands (which contribute for about 10% of the total band intensity) or to minor isotopic species present in the sample in natural abundance.

The analysis was initiated by following series of regular patterns in the P branch. Examples of such rather regular series are given in Fig. 2. The ground state energy levels were calculated using the ground state parameters of Ref. [5] and added to the measured line positions to get the experimental upper state energy levels. These upper state levels were introduced in a least-squares fit in order to get a first set of upper state parameters (vibrational energy and rotational and spin- rotational constants) for the (4,0,1) state. Then, a preliminary synthetic spectrum of the $4\nu_1+\nu_3$ band was generated which allowed for new assignments. The initial energy level calculations were performed considering only the spin-rotation interactions within the (4,0,1) vibrational state, but at a given step of the analysis, it was necessary to include vibration-rotation interactions involving the energy levels of the (4,0,1) state with

those of the (4,2,0) and (0,9,0) dark vibrational states. This process was repeated iteratively until no more lines could be assigned.

The search for extra lines from the dark $4\nu_1+2\nu_2$ and $9\nu_2$ dark bands was unsuccessful because of the spectral congestion of the CRDS spectrum due to hot bands, minor isotopic species or impurities (see Fig. 3 for example). The final results of the analysis are summarized in Table 1. Overall 532 energy levels could be derived. They are provided as Supplementary Material.

3.2. Energy level calculation

The first energy levels calculation were performed accounting for the spin-rotation interactions within both (4,0,1) and (4,2,0) together with the vibration-rotation resonances involving energy levels from the (4,0,1) bright state with those from the (4,2,0) dark state. Indeed, this Coriolis-type resonance, which involves the $(v_1,v_2,v_3) \Leftrightarrow (v_1,v_2\pm2,v_3\mp1)$ resonating vibrational states, is commonly encountered in the NO_2 molecule [6, 8-11, 15]. However, it was impossible to reproduce the (4,0,1) energy levels for $N\geq35$ or $K_a\geq4$. In addition for $K_a=0$ and $5\leq N \leq19$, the calculated energy are shifted relative to the observed ones by about 0.01 cm^{-1}. This leads to apparent overestimated intensities in the 6645-6650 and 6680-6686 cm^{-1} of the P and R-branches, respectively which is apparent on the upper panel of Fig. 1. It was clear that additional vibration-rotation resonances had to be taken into account.

The list of the dark vibrational states [16] possibly interacting with the (4,0,1) bright state is presented in Table 2. Depending on the symmetry of the (v_1,v_2,v_3) dark state, the $(v_1,v_2,v_3) \leftrightarrow$ (4,0,1) resonance coupling may be anharmonic (for odd values of v_3) or C-type Coriolis (for even values of v_3). We investigated one by one all the possible resonance interactionsn

High order anharmonic resonances may play an important role. For instance, Delon et al introduced the $(v_1, v_2, v_3) \leftrightarrow (v_1 \mp 3, v_2 \pm 1, v_3 \pm 2)$ coupling in the effective vibrational Hamiltonian that they developed to reproduce the complete set of 191 vibrational levels up to 10000 cm^{-1} Ref. [16]. Accordingly, the possible existence of the (4,0,1) ↔ (1,1,3) anharmonic resonance was considered in the present analysis, but without success.

Finally, it appeared that the dark state at 6705.23 cm^{-1}, identified as (0,9,0) in Ref. [16], is responsible for most of the observed additional perturbations. Therefore, three interacting states {(4,2,0), (0,9,0), (4,0,1)} are involved in the final modeling which used the Hamiltonian matrix given in Table 3. This final calculation takes explicitly into account the electron spin-rotation interactions within each of the (4,2,0), (0,9,0) and (4,0,1) vibrational states together with the (4,2,0) ↔ (4,0,1) and (0,9,0) ↔ (4,0,1) Coriolis type interactions and an anharmonic resonance linking the (4,2,0) and (0,9,0) energy levels.

The 532 spin-rotation energy levels of the (4,0,1) state obtained in this work, together with the experimental vibrational energy of the (4,2,0) and (0,9,0) states [16] were introduced at their estimated uncertainty in a least-squares calculation to fit the parameters of the upper {(4,2,0), (0,9,0), (4,0,1)} interacting states. The vibrational energies and rotational, spin-rotational and coupling constants deduced from the fit together with their estimated uncertainties are listed in Table 4. Only some of the rotational and spin-rotational constants could be fitted for the (4,2,0) and (0,9,0) dark states, the other ones being fixed to their ground state values [5].

The results of the energy levels calculations proved to be rather satisfactory, as can be seen from the standard deviation (2.4×10^{-3} cm^{-1}) and statistical analysis given in the lower part of Table 1. However, the (obs.-calc.) values included in the Supplementary Material show that some (4,0,1) spin-rotation energy levels could not be reproduced within their experimental uncertainty (on the order of 1.0×10^{-3} cm^{-1}). This may be the result of a lack of information relative to the (4,2,0) and (0,9,0) dark states, except for the LIDFS vibrational energies [16].

The fitted value of the vibrational energy of the (4,0,1) state (E_{401}=6676.8796(14)cm^{-1}) is very close to the LIDFS value (E_{401} = 6676.86 cm^{-1}) Ref. [16].

The ν_2 vibrational mode is associated with the NO_2 bending mode and according to the vibration-rotation parameters derived from microwave studies [22], the A rotational constant is expected to increase significantly with the ν_2 vibrational quantum number. For example, the experimental values of the $A_{0\nu_2 0}$ progression are A_{000} = 8.00235469 cm^{-1} [5], A_{010} = 8.37412738 cm^{-1} [4], A_{020} = 8.7787058 cm^{-1} [7], A_{030} = 9.20316 cm^{-1} [8], A_{040} = 9.8075 cm^{-1} [9], A_{080} = 12.45212 cm^{-1} [15], respectively. Our fitted values of the A rotational constant of the (0,9,0) and (4,2,0) vibrational states (A_{090}=10.6259(25) and A_{420}=12.3059(67) cm^{-1}), differ significantly from the values extrapolated using the A_e equilibrium rotational constant and the ${}^{A}\alpha_i^0$ and ${}^{A}\gamma_{ij}$ (first and second order, respectively) vibration-rotation constants derived in Ref. [22] ($^{\text{Predicted}}A_{090}$ ~ 12.5 cm^{-1} and $^{\text{Predicted}}A_{420}$ ~ 9.3 cm^{-1}). Nevertheless, we note that the predicted variation of the *sum* of the A rotational constants $^{\text{Predicted}}(A_{090}+A_{420}-2\times A_{000})$~ 5.8 cm^{-1} is in good agreement with the experimental value ~ 6.9 cm^{-1}. It indicates that the (0,9,0) and (4,2,0) dark states are strongly mixed by anharmonic resonances and that the fitted values of their A rotational constants are highly correlated.

Therefore, and contrary to what could be done in Ref. [15], the fitted values of the rotational constant cannot be used to confirm the (0,9,0) and (4,2,0) vibrational assignments proposed in Ref. [16] for the states located at 6705.23 cm^{-1} and 6653.54 cm^{-1}.

Let us consider in more details the interactions between the energy levels of the {(4,2,0), (0,9,0), (4,0,1)} triad.

<u>The (0,9,0) ⇔ (4,2,0) anharmonic resonance</u>

The quality of the least squares fit calculation was significantly improved by including a weak but significant anharmonic interaction in N_z^2 linking the (0,9,0) and (4,2,0) vibrational energy

levels. More explicitly, the K_a=4-6 energy levels of the (0,9,0) ⇔ (4,2,0) interacting states are strongly mixed (up to 50% for K_a=6) within a ΔK_a=0 resonance.

The (0,9,0) ⇔ (4,0,1) and (4,2,0) ⇔ (4,0,1) Coriolis resonances:

This resonance interaction connects the K_a = 7 energy levels of the (4,0,1) state to the K_a = 6 levels of the (0,9,0) and (4,2,0) dark states. Both dark states are contributing to this interaction because their K_a = 6 series are themselves strongly mixed by anharmonic resonances and the dominant contribution cannot be discriminated. The mixing coefficient of the rotational levels of the (4,2,0) dark state reaches its maximum of 45% at N' around 12.

In addition, for odd N values, the K_a = 1 energy levels of the (4,0,1) state are resonating with the [N, K_a=2, K_c=N-1] levels of the (4,2,0) dark state. In this case, the resonance reaches its maximum at N=35.

In Ref. [15], an unexpected Coriolis resonance involving the (0,8,0) and (1,0,3) resonating states was pointed out for the first time. This was a surprise for NO_2 because the interacting vibrational states differ by twelve vibrational quanta.

In the present study, the existence of a strong anharmonic resonance coupling the (0,9,0) and (4,2,0) dark states provides a partial explanation to the existence of C-type Coriolis resonances coupling the (4,0,1) state to both (0,9,0) and (4,2,0) states.

The high order resonances evidenced in the $\nu_1+3\nu_3$ band [15] and in the present study of the $4\nu_1+\nu_3$ band show that the description of the vibrational states in the classical normal mode scheme begins to fail for vibrational excitations higher than 5900 cm^{-1}.

3.3. Line intensities and synthetic spectrum

Except for UV-VIS cross sections in the 10000–42000 cm^{-1} spectral range [23], to the best of our knowledge, no quantitative intensities measurements are available for nitrogen dioxide above 5000 cm^{-1}.The intensities of 64 individual lines of the $4\nu_1+\nu_3$ line were measured by

using a multiline fitting program and assuming a Voigt line profile. Considering the congestion of the spectrum and the uncertainty associated with the estimation of the NO_2 partial pressure in the sample, we estimate to 20 % the uncertainty on the reported absolute values of the intensities. For these measurements, taking into account the partial pressure of the dimer (N_2O_4) and the isotopic abundance (a_{Main}=0.991616 [24]), the partial pressure of the main $^{14}N^{16}O_2$ isotopic species is estimated to be P= 8.9 Torr .

The method used to compute NO_2 line intensities was extensively described in Refs. [3, 6] and only the relevant points are recalled here. The intensity of a line $k_{\tilde{\nu}}^{N}$ for a pure $^{14}N^{16}O_2$ isotopic sample is given (in cm^{-1}/(molecule cm^{-2})) by:

$$k_{\tilde{\nu}}^{N} = \frac{8\pi^3\tilde{\nu}}{3hc4\pi\varepsilon_0}\left(\exp\left(-\frac{E_L}{kT}\right)-\exp\left(-\frac{E_U}{kT}\right)\right)\frac{g_L}{Z(T)}R_L^U. \qquad (2)$$

In this expression E_L and E_U are the lower and upper levels of the transition, and $\tilde{\nu}=(E_U-E_L)/hc$ is the wavenumber of the transition. $Z(T)=Z_{vib}(T)\times Z_{rot}(T)$ is the total partition function including the nuclear spin contribution ($g_L = 2I+1=3$ for $^{14}N^{16}O_2$). According to Refs. [3,6], Z(296 K) = 13618 which is in reasonable agreement with the HITRAN value [13]. The transition moment is expressed as:

$$R_L^U = \left|\left\langle V^U, N^U K_a^U K_c^U S J^U \left|\mu_Z^{'}\right| V^L, N^L K_a^L K_c^L S J^L \right\rangle\right|^2, \qquad (3)$$

where U and L refer to upper and lower state, respectively. The vibrational state is denoted by $V=|v_1,v_2,v_3\rangle$ and $\mu_Z^{'}$ is the transformed dipole-moment operator of the $4\nu_1+\nu_3$ band, which for an A-type band takes the following form:

$$^{(000)(401)}\mu_Z^{'} = {}^{(000)(401)}\mu_a\,\varphi_z \qquad (4)$$

where φ_z represents the direction cosines Φ_z. Indeed it appeared that the whole set of line intensities could be reproduced without taking into account higher order rotational operators (Herman Wallis type) in the expansion of the transition moment operator.

In this condition, the $4\nu_1+\nu_3$ line intensities are proportional to $\left|{}^{(000)(401)}\mu_a\right|^2$ and the absolute value of the ${}^{(000)(401)}\mu_a$ constant:

$$|{}^{(000)(401)}\mu_a| = 2.3\times10^{-4}\ (\pm10\ \%)\ \text{Debye} \quad (5)$$

was determined through a least squares fit performed on the set of the experimental intensities values (see Table 5). The comparison of the observed and calculated intensities included in Table 5 shows a satisfactory agreement.

Using the vibrational energies and rotational, spin-rotational, and coupling constants given in Table 3 for the upper resonating {(4,2,0), (0,9,0), (4,0,1)} vibrational states and the parameters in Ref. [5] for the ground (000) vibrational state, a comprehensive list of line positions was generated for the $4\nu_1+\nu_3$ band. Since several perturbations due to (4,2,0) and (0,9,0) dark states are not accounted for correctly in our calculation (see the discussion in section 3), the line positions were adjusted whenever possible, using the experimentally determined values of the (4,0,1) upper levels (see Supplementary Materials). The line intensities were computed using the value of the ${}^{(000)(401)}\mu_a$ constant given in Eq.(5).

The calculation was performed at 296 K using an intensity cut-off of 1×10^{-28} cm^{-1}/(molecule cm^{-2}), as well as maximum values of 61 for N and 9 for K_a. The synthetic spectrum including 4893 lines between 6556 and 6915 cm^{-1} is provided as Supplementary Material..

The resulting calculated integrated band intensities (at 296 K) are S_{401}= 1.37×10^{-21} cm^{-1}/(molecule cm^{-2}), S_{420} = 0.35×10^{-24} cm^{-1}/(molecule cm^{-2}) and S_{090} = 0.32×10^{-23} cm^{-1}/(molecule cm^{-2}) for the $4\nu_1+\nu_3$, $4\nu_1+2\nu_2$ and $9\nu_2$ bands, respectively.

Finally, it is possible to get an estimation of the band intensity by estimating the hot bands contribution in the harmonic approximation through the usual expression:

$$S_{1.5\mu m} = Z_{vib}(296\ K)\times(\ S_{401} + S_{420} + S_{090}) \quad (6)$$

with Z_{vib}(296 K) = 1.029 [12]. In this way the value $S_{1.5\ \mu m}$ (296K)= 1.45 $\times 10^{-21}$ cm^{-1}/(molecule cm^{-2}) is obtained.

The experimental and calculated spectra of the $4\nu_1+\nu_3$ band of NO_2 are compared in Figs. 1–5. An overview of the $4\nu_1+\nu_3$ band and a portion of the P branch near 6263.5 cm^{-1} are presented in Fig. 1 and Fig. 2, respectively. Fig. 3 shows a section of the low frequency range of the P branch: in this region lines involving rather high N and K_a values are observable (N=34 and 35 and $K_a \leq 8$). In Figs. 4 and 5, the comparison is displayed for the congested Q and R branches, respectively. In all cases, the agreement between the observed and calculated spectra is very good, confirming the quality of the calculation.

4. Conclusion

The high-resolution Cavity Ring Down laser spectrum of nitrogen dioxide was recorded near 1.5 μm which allowed the first extensive analysis of the $4\nu_1+\nu_3$ band of $^{14}N^{16}O_2$. This band is the highest combination band of nitrogen dioxide in the X^2A_1 ground state, analyzed so far at high-resolution. A Hamiltonian matrix which accounts for Coriolis, electron spin-rotation and anharmonic interactions was constructed for the determination of the experimental spin-rotation energy levels of the {(4,2,0), (0,9,0), (4,0,1)} interacting states of NO_2. Using the reproduced energy levels a comprehensive list of line positions and of reasonably estimated line intensities of the $4\nu_1+\nu_3$ band of $^{14}N^{16}O_2$ has been generated.

Acknowledgments

A.P. is grateful to the INSU (Institut national des sciences de l'Univers) of the CNRS for financial support.

References

[1] Lopez-Puertas M, Funke B, Von Clarmann T, Fischer H, Stiller GP. The stratospheric and mesospheric NO_y in the 2002-2004 polar winters as measured by MIPAS/ENVISAT. Space Sci Rev 2006;125:403–416.

[2] Notholt J, Toon GC, Lehmann R, Sen B, Blavier, JF. Comparison of Arctic and Antarctic trace gas column abundances from ground-based Fourier transform infrared spectrometry. J Geophys Res 1997;102:12863–12869.

[3] Perrin A, Flaud JM, Camy-Peyret C, Carli B, Carlotti M, The far infrared spectrum of NO_2-Electron spin resonance and hyperfine Fermi contact resonance in the ground state, Mol. Phys. 63 (1988) 791–810.

[4] Perrin A, Camy-Peyret C, Flaud JM, Kauppinen J, The ν_2 band of NO_2: line positions and intensities , J Mol Spectrosc 1988; 130: 168–182.

[5] Semmoud-Monnanteuil N, Colmont JM, Perrin A, Flaud JM, Camy-Peyret C, New measurements in the millimeter wave spectrum of NO_2, J Mol Spectrosc 134 (1989) 176–182.

[6] Perrin A, Flaud JM, Camy-Peyret C, Vasserot AM, Guelachvili G, Goldman A, Murcray FJ, Blatherwick RD, The $(\nu_1,2\nu_2,\nu_3\}$ interacting bands of NO_2: line positions and intensities. J Mol Spectrosc 1992;154:391–406.

[7] Perrin A, Flaud JM, Camy-Peyret C, Goldman A, Murcray JF, Blatherwick RD, Rinsland CP, The ν_2 and $2\nu_2-\nu_2$ bands of $^{14}N^{16}O_2$: electron spin-rotation and hyperfine contact resonances in the (010) vibrational state. J Mol Spectrosc 1993;160: 456–463.

[8] Perrin A, Flaud JM, Camy-Peyret C, Hurtmans D, Herman H, Guelachvili G, The $\nu2+\nu3$ and the $\nu_2+\nu_3-\nu_2$ bands of NO_2: line positions and intensities, J Mol Spectrosc 1994;168: 54–66.

[9] Perrin A, Flaud JM, Camy-Peyret C, Hurtmans D, Herman H, The $\{2\nu3, 4\nu2,2\nu3+\nu_3\}$ and $2\nu_2-\nu_2$ bands of NO_2 : line positions and line intensities. J Mol Spectrosc 1996; 177: 58–65.

[10] Mandin JY, Dana V, Perrin A, Flaud JM, Camy-Peyret C, Régalia L, Barbe A, The $\{\nu_1+ 2\nu_2,\nu_1+ \nu_3\}$ bands of NO_2: line positions and intensities; line intensities in the $\nu_1+ \nu_2 +\nu_3- \nu_2$ hot band. J Mol Spectrosc 1997;181: 379–388.

[11] Stephen TM, Goldman A, Perrin A, Flaud JM, Keller F, Rinsland CP, New high resolution analysis of the $3\nu_3$ and $2\nu_1+\nu_3$ bands of nitrogen dioxide (NO_2) by Fourier transform transform spectroscopy, J Mol Spectrosc 2000; 201: 134–142.

[12] Perrin A, Flaud JM, Camy-Peyret C, W.J. Lafferty, Ph. Arcas, Rinsland CP, NO_2 and SO_2 line parameters: 1996 HITRAN update and new results. JQSRT 1998;60: 839–850.

[13] Rothman LS, Gordon IE, Barbe A, Benner DC, Bernath PF, Birk M, Boudon V, Brown LR, Campargue A, Champion JP, Chance K, Coudert LH, Dana V, Devi VM, Fally S, Flaud JM**,** Gamache RR, Goldman A, Jacquemart D, Kleiner I, Lacome N, Lafferty WJ, Mandin JY, Massie ST, Mikhailenko SN, Miller CE, Moazzen-Ahmadi N, Naumenko OV, Nikitin AV, Orphal J, Perevalov VI, Perrin A, Predoi-Cross A, Rinsland CP, Rotger M, Simeckova M, Smith MAH, Sung K, Tashkun SA, Tennyson J, Toth RA, Vandaele AC, Vander Auwera J, The HITRAN 2008 molecular spectroscopic database. JQSRT 2009; 110: 533-572.

[14] Jacquinet-Husson N, Scott NA, Chédin A, Crépeau L, Armante R, Capelle V, Orphal J, Coustenis A, Barbe A, Birk M, Brown LR, Camy-Peyret C, Claveau C, Chance K, Christidis N, Clerbaux C, Coheur PF, Dana V, L. Daumont, M.R. Debacker-Barilly, Di Lonardo G, Flaud JM, Goldman A, Hamdouni A, Hess M, Hurley MD, Jacquemart D, Kleiner I, Köpke

P, Mandin JY, Massie S, Mikhailenko S, Nemtchinov V, Nikitin A, Newnham D, Perrin A, Perevalov VI, Pinnock S, Régalia-Jarlot L, Rinsland CP, Rublev A, Schreier F, Schult L, Smith KM, Tashkun SA, Teffo JL, Toth RA, Tyuterev VIG, Vander Auwera J, Varanasi P, Wagner G, The GEISA spectroscopic database: Current and future archive for Earth's planetary atmosphere studies", JQSRT 2008; 109:1043-1059.

[15] Miljanic S, Perrin A, Orphal J, Fellows CE, Chelin P, "New high resolution analysis of the $\nu_1+3\nu_3$ band of nitrogen dioxide", J Mol Spectrosc 2008;251: 9-15.

[16] Delon A, Jost R, Laser induced dispersed fluorescence spectra of jet cooled NO_2: The complete set of vibrational levels up to 10 000 cm^{-1} and the onset of the X^2A_1-$A^{*2}B_2$ vibronic interaction. J Chem Phys 1991;95: 5686–5700.

[17] R.E. Blank, C.D. Hause, Molecular constants for the (3,0,1) state of NO_2. J Mol Spectrosc 1970;34: 478-486.

[18] Macko P, Romanini D, Mikhailenko SN, Naumenko OV, Kassi S, Jenouvrier A, et al. High sensitivity CW-cavity ring down spectroscopy of water in the region of the 1.5 μm atmospheric window. J Mol Spectrosc 2004;227:90-108.

[19] Morville J, Romanini D, A.A. K, M. C. Two schemes for trace detection using cavity ringdown spectroscopy. Appl Phys 2004;D78:465-76.

[20] Perevalov BV, Kassi S, Romanini D, Perevalov VI, Tashkun SA, Campargue A. CW-cavity ringdown spectroscopy of carbon dioxide isotopologues near 1.5 μm. J Mol Spectrosc 2006;238:241-55.

[21] Hurtmans D, Herman M, and Vander Auwera J, Integrated band intensities in N_2O_4 in the infrared range. JQSRT 1993;50:595-602.

[22] Morino Y, Tanimoto M, Saito S, Hirota E, Awata R, Tanaka T, Microwave Spectrum of Nitrogen Dioxide in Excited Vibrational States-Equilibrium Structure. J Mol Spectrosc 1983; 98:331–348.

[23] Orphal J, Chance K, Ultraviolet and visible absorption cross-sections for HITRAN. JQSRT 2003;82: 491-504.

[24] De Bievre P, Holden NE, and Barnes IL, Isotopic Abundances and Atomic Weights of the Elements. J Phys Chem Ref Data 1984;13**:**809-891.

List of Tables

Table 1

Range of the observed energy levels and statistical analysis of the results of the energy levels calculation.

Table 2

List of the vibrational states located nearby the (4,0,1) vibrational state.

Caption: The symmetry of the vibrational state (A_1 or B_1) depends on the v_3 parity (even or odd).

[#]Ref. [16], $ This work

Table 3

Hamiltonian matrix for the {(4,2,0), (0,9,0), (4,0,1)} interacting vibrational states of NO_2

Table 4

Vibrational energies, rotational, spin-rotational, and coupling constants for the {(4,2,0), (0,9,0), (4,0,1)} interacting vibrational states of NO_2

Note. The results are in cm^{-1} and the quoted errors correspond to one standard deviation.

[a] From Ref. [5].

Constants marked with # were held fixed to the ground state values [5].

Table 5

List of line intensities measured for the $4\nu_1+\nu_3$ band of NO_2.

The first and second columns give the calculated line position and intensities, the upper and lower rotational N, K_a and K_c quantum numbers. In the J columns, + and – stand for J=N+1/2 and J=N-1/2, respectively. The last two columns give the experimental line positions and intensities.

The intensities are given in 10^{-24} $cm^{-1}/(molecule.cm^{-2})$ at 296K.

$ For the unresolved doublets, the total line intensity is given.

Figure captions

Fig. 1. Overview of the absorption spectrum of nitrogen dioxide in the 6620-6700 cm^{-1} spectral range. In both panels, the CRDS spectrum (upper trace) and the calculated spectra (lower trace) are displayed. A small section of the experimental spectrum around 6655 cm^{-1} is not displayed because it shows a number of saturated lines. The agreement between the observed and calculated spectra is significantly better when both the (0,9,0)⇔(4,0,1) and (4,2,0)⇔(4,0,1) Coriolis resonances are taken into account ("full calc", in the lower panel) than when only the (4,2,0)⇔(4,0,1) Coriolis resonances are considered (upper panel). The sample pressure of the CRDS spectrum was 10.0 Torr.

Fig. 2. Portion of the P branch of the $4\nu_1+\nu_3$ band in the 6669 cm^{-1} region.
Upper trace: experimental spectrum. *Lower trace*: calculated spectrum. The assignments are for the upper state *N* and K_a values. For $K_a \geq 4$, the lines are split in two spin-rotation subcomponents noted by a black and open triangle for $J=N-1/2$ and $J=N+1/2$, respectively.

Fig.3. Portion of the P branch of the $4\nu_1+\nu_3$ band in the 6631.5 cm^{-1} region
The assignments are given for the upper N' values. For $K_a=0$ and 1, the observed spin-rotation splittings are indicated by open and black triangles for $J' = N' + 1/2$ and $J' = N' - 1/2$, respectively.

Fig. 4. Portion of the Q branch of the $4\nu_1+3\nu_3$ band in the 6676.5 cm^{-1} region.
The assignments for the ${}^{Q}Q_{K_a=3}$ subranch are given. Excellent agreement between the experimental and calculated lines is observed.

Fig. 5. Portion of the R branch of the $4\nu_1+\nu_3$ band in the 6690 cm^{-1} region.
The *N*' (upper level) values are given for the ${}^{Q}R_{K_a=0}$ series of transitions.

Table 1

$4\nu_1+3\nu_3$ band	
1105 lines $N \le 49$, $K_a \le 8$	
Statistical analysis of the results	
Number of spin-rotation levels:	532
$0 \le \delta \le 0.005$ cm^{-1}	65.1 %
$0.005 \le \delta \le 0.010$ cm^{-1}	19.5 %
$0.010 \le \delta \le 0.020$ cm^{-1}	8.9 %
$0.020 \le \delta \le 0.040$ cm^{-1}	5.4 %
Standard deviation: 0.24×10^{-2} cm^{-1}	

$\delta = |E_{obs} - E_{calc}|$

Table 2

$(v_1\ v_2\ v_3)$ **Sym.**	E_v
(1,3,2) $\mathbf{A_1}$	6616.53[#]
(4,2,0) $\mathbf{A_1}$	6653.54[#]
(4,0,1) $\mathbf{B_1}$	6676.882 [$]
(1,1,3) $\mathbf{B_1}$	6693.12 [#]
(0,9,0) $\mathbf{A_1}$	6705.23[#]
(0 ,7,1) $\mathbf{B_1}$	6761.44[#]

[#]Ref. [16]
$ This work

Table 3

Hamiltonian matrix

		J					
		(4,2,0)		**(0,9,0)**		**(4,0,1)**	
		N=J-1/2	**N=J+1/2**	**N=J-1/2**	**N=J+1/2**	**N=J-1/2**	**N=J+1/2**
(4,2,0)	**N=J-1/2**	$H_{vv}+V_{vv}^{SR}$	V_{vv}^{SR}	$H_{vv'}^{Anh}$		$H_{vv'}^{C}$	
	N=J+1/2	V_{vv}^{SR}	$H_{vv}+V_{vv}^{SR}$		$H_{vv'}^{Anh}$		$H_{vv'}^{C}$
(0,9,0)	**N=J-1/2**	$H_{vv'}^{Anh}$		$H_{vv}+V_{vv}^{SR}$	V_{vv}^{SR}	$H_{vv'}^{C}$	
	N=J+1/2		$H_{vv'}^{Anh}$	V_{vv}^{SR}	$H_{vv}+V_{vv}^{SR}$		$H_{vv'}^{C}$
(4,0,1)	**N=J-1/2**	$H_{vv'}^{C}$		$H_{vv'}^{C}$		$H_{vv}+V_{vv}^{SR}$	V_{vv}^{SR}
	N=J+1/2		$H_{vv'}^{C}$		$H_{vv'}^{C}$	V_{vv}^{SR}	$H_{vv}+V_{vv}^{SR}$

H_{vv} : Watson's A-type I^r representation Hamiltonian

$$
\begin{aligned}
H_{vv} = {} & E_v + \left[A^v - \frac{1}{2}\left(B^v + C^v\right) \right] N_z^2 + \frac{1}{2}\left(B^v + C^v\right) \mathbf{N}^2 + \frac{1}{2}\left(B^v - C^v\right) N_{xy}^2 \\
& - \Delta_K^v N_z^4 - \Delta_{JK}^v N_z^2 \mathbf{N}^2 - \Delta_J^v \left(\mathbf{N}^2\right)^2 - \delta_K^v \left\{ N_z^2, N_{xy}^2 \right\} - 2\delta_J^v N_{xy}^2 \mathbf{N}^2 \\
& + H_K^v N_z^6 + H_{KJ}^v N_z^4 \mathbf{N}^2 + H_{JK}^v N_z^2 \left(\mathbf{N}^2\right)^2 + H_J^v \left(\mathbf{N}^2\right)^3 \\
& + h_K^v \left\{ N_z^4, N_{xy}^2 \right\} + h_{KJ}^v \left\{ N_z^2, N_{xy}^2 \right\} \mathbf{N}^2 + 2h_J^v N_{xy}^2 \left(\mathbf{N}^2\right)^2 + \ldots
\end{aligned}
$$

V_{vv}^{SR} : Electron-spin rotation interactions

$$
\begin{aligned}
V_{vv}^{SR} = {} & \varepsilon_{aa}^v S_a N_a + \varepsilon_{bb}^v S_b N_b + \varepsilon_{cc}^v S_c N_c + \Delta_N^{vS} (\mathbf{N}\cdot\mathbf{S}) + \frac{1}{2}\Delta_{NK}^{vS} \left\{ \mathbf{N}^2 N_z S_z + S_z N_z \mathbf{N}^2 \right\} + \Delta_{KN}^{vS} N_z^2 (\mathbf{N}\cdot\mathbf{S}) \\
& + \Delta_K^{vS} N_z^3 S_z + \delta_N^{vS} \left(N_+^2 + N_-^2\right)(\mathbf{N}\cdot\mathbf{S}) + \frac{1}{2}\delta_K^{vS} \left\{ \left(N_+^2 + N_-^2\right) N_z S_z + N_z S_z \left(N_+^2 + N_-^2\right) \right\}
\end{aligned}
$$

$H_{vv'}^{C}$: Coriolis-type interactions

$$
H_{vv'}^{C} = h_{vv'}^{1C} i N_y + h_{vv'}^{2C} i N_y N_z^2 + h_{vv'}^{3C} i N_y \mathbf{N}^2 + h_{vv'}^{4C} \left\{ N_x, N_z \right\} + h_{vv'}^{5C} \left\{ \left\{ N_x, N_z \right\}, N_z^2 \right\} + h_{vv'}^{6C} \left(N_-^3 - N_+^3 \right), \ldots
$$

$H_{vv'}^{Anh}$: Anharmonic interactions

$$
H_{vv'}^{Anh} = h_{vv'}^{1Anh} \mathbf{N}_z^2 + h_{vv'}^{2Anh} \mathbf{N}_{xy}^2
$$

Table 4

	(000)[a]	(4,2,0)	(0,9,0)	(4,0,1)
Band centers and rotational constants				
E_v		6653.543(24)	6705.238(24)	6676.8796(14)
A	8.00235469	12.30591(670)	10.62589(250)	8.028063(290)
B	0.433706798	0.42376(140)	0.410771(700)	0.42153980(750)
C	0.410442540	0.38947(150)	0.410021(680)	0.39703484(860)
Δ_K	0.26878757×10^{-2}	#	#	$0.36367(130)\times10^{-2}$
Δ_{KN}	-0.196822×10^{-4}	#	#	$-0.42819(700)\times10^{-4}$
Δ_N	0.2992447×10^{-6}	$3.774(250)\times10^{-6}$	#	$0.37063(220)\times10^{-6}$
δ_K	0.40547×10^{-5}	#	#	$-7.143(240)\times10^{-5}$
δ_N	0.3192774×10^{-7}	#	#	$1.0389(170)\times10^{-7}$
H_K	0.303157×10^{-5}	#	#	$0.1412(170)\times10^{-5}$
H_{KN}	-0.270439×10^{-7}	#	#	#
H_{NK}	0.2995×10^{-10}	#	#	#
H_N	0.2866×10^{-12}	#	#	#
h_K	0.29297×10^{-7}	#	#	$-48.381(500)\times10^{-7}$
h_{KN}	-0.3637×10^{-10}	#	#	#
h_N	0.1057×10^{-12}	#	#	#
L_K	-0.51104×10^{-8}	#	#	#
L_{KKN}	0.35117×10^{-10}	#	#	#
L_{KN}	0.12158×10^{-12}	#	#	#
P_K	0.867×10^{-11}	#	#	#
Q_K	-0.8439×10^{-14}	#	#	#
Spin-rotational constants				
ε_{aa}^{v}	0.180353006	0.19377(114)	0.4146(126)	0.158213(105)
ε_{bb}^{v}	0.257833×10^{-3}	#	#	$0.3077(267)\times10^{-3}$
ε_{cc}^{v}	-0.3178107×10^{-2}	#	#	$-0.31740(284)\times10^{-2}$
Δ_K^{vS}	-0.17606×10^{-3}	#	#	#
$\Delta_{KN}^{vS}+\Delta_{NK}^{vS}$	0.6005×10^{-6}	#	#	#
Δ_N^{vS}	0.6322×10^{-9}	#	#	#
Δ_{NK}^{vS}	0.1678×10^{-5}	#	#	#
δ_K^{vS}	0.3769×10^{-6}	#	#	#
δ_N^{vS}	0.244×10^{-9}	#	#	#
H_K^S	0.29673×10^{-6}	#	#	#
L_K^S	-0.3569×10^{-9}	#	#	#

$H^{C}_{vv'}$: Coriolis-type interactions

$$H^{C}_{vv'} = h^{1C}_{vv'} i N_y + h^{2C}_{vv'} i N_y N_z^2 + h^{3C}_{vv'} i N_y \mathbf{N}^2 + h^{4C}_{vv'} \left\{ N_x, N_z \right\} + h^{5C}_{vv'} \left\{ \left\{ N_x, N_z \right\}, N_z^2 \right\} + h^{6C}_{vv'} \left(N_-^3 - N_+^3 \right), ...$$

Coupling constants		
Coriolis:	(4,2,0) ⇔ (4,0,1)	(0,9,0) ⇔ (4,0,1)
$i N_y$	-0.3327(150)×10^{-1}	-0.32673(500)×10^{-1}
$\left\{ i N_y, N_z^2 \right\}$	0.2737(100)×10^{-2}	
$i N_y \mathbf{N}^2$	0.1875(110)×10^{-4}	
$\left\{ N_x, N_z \right\}$	-0.2007(400)×10^{-2}	
$\left\{ \left\{ N_x, N_z \right\}, N_z^2 \right\}$	-0.52470(720)×10^{-3}	
$\left(N_-^3 - N_+^3 \right)$	-0.45871(530)×10^{-4}	
Anharmonic:	(4,2,0) ⇔ (0,9,0)	
$\mathbf{N}_z^2$	-0.90409(170)	
$\mathbf{N}_{xy}^2$	0.1835(390)×10^{-2}	

Table 5

Sig calc	Int-calc [#]	N'	K_a'	K_c'	J'	N"	K_a"	K_c"	J"	Sig exp	Int Exp [#]	
6638.8888	1.32	30	1	30	+	31	1	31	+	6638.8911	1.29	
6642.1080	1.58	28	1	28	+	29	1	29	+	6642.1076	1.54	
6642.1183	1.52	28	1	28	-	29	1	29	-	6642.1200	1.66	
6645.2195	1.85	26	1	26	+	27	1	27	+	6645.2180	2.16	
6646.5887	1.84	25	1	24	-	26	1	25	-	6646.5893	3.61	$
6646.5899	1.91	25	1	24	+	26	1	25	+			
6646.7659	1.67	25	2	23	-	26	2	24	-	6646.7675	3.01	$
6646.7674	1.73	25	2	23	+	26	2	24	+			
6649.5247	2.10	23	1	22	-	24	1	23	-	6649.5254	4.34	$
6649.5259	2.19	23	1	22	+	24	1	23	+			
6649.6126	2.21	23	0	23	-	24	0	24	-	6649.6154	4.37	$
6649.6150	2.31	23	0	23	+	24	0	24	+			
6649.7020	1.89	23	2	21	-	24	2	22	-	6649.7028	4.30	$
6649.7022	1.97	23	2	21	+	24	2	22	+			
6652.3577	2.33	21	1	20	-	22	1	21	-	6652.3586	4.04	$
6652.3589	2.44	21	1	20	+	22	1	21	+			
6652.4513	2.46	21	0	21	-	22	0	22	-	6652.4510	5.02	$
6652.4535	2.57	21	0	21	+	22	0	22	+			
6656.6077	2.66	18	1	18	-	19	1	19	-	6656.6104	6.37	$
6656.6106	2.80	18	1	18	+	19	1	19	+			
6656.6266	2.33	18	2	17	-	19	2	18	-	6656.6291	3.99	$
6656.6300	2.46	18	2	17	+	19	2	18	+			
6660.3300	2.86	15	0	15	-	16	0	16	-	6660.3341	5.29	$
6660.3341	3.05	15	0	15	+	16	0	16	+			
6662.6807	2.70	13	1	12	-	14	1	13	-	6662.6819	4.60	$
6662.6823	2.90	13	1	12	+	14	1	13	+			
6662.7567	2.83	13	0	13	-	14	0	14	-	6662.7570	5.09	$
6662.7585	3.04	13	0	13	+	14	0	14	+			
6662.8660	2.39	13	2	11	-	14	2	12	-	6662.8697	5.42	$
6662.8707	2.57	13	2	11	+	14	2	12	+			
6663.0024	1.90	13	3	10	-	14	3	11	-	6663.0029	3.74	$
6663.0032	2.05	13	3	10	+	14	3	11	+			
6666.4489	1.70	10	3	8	-	11	3	9	-	6666.4500	1.89	
6666.4578	1.86	10	3	8	+	11	3	9	+	6666.4588	1.52	
6667.5475	1.58	9	3	6	-	10	3	7	-	6667.5483	1.39	
6667.5580	1.75	9	3	6	+	10	3	7	+	6667.5603	1.42	
6668.6183	1.44	8	3	6	-	9	3	7	-	6668.6197	1.53	
6669.6859	1.45	7	3	4	+	8	3	5	+	6669.6858	1.52	
6671.5761	1.48	5	2	3	+	6	2	4	+	6671.5762	1.64	
6681.3566	1.85	6	1	6	+	5	1	5	+	6681.3553	1.64	
6681.3658	1.56	6	1	6	-	5	1	5	-	6681.3647	1.47	
6681.5376	1.51	6	2	5	+	5	2	4	+	6681.5375	1.70	
6682.6338	2.05	8	1	8	-	7	1	7	-	6682.6315	2.38	

6682.8468	1.98	8	2	7	+	7	2	6	+	6682.8456	2.29
6682.8629	1.75	8	2	7	-	7	2	6	-	6682.8611	1.69
6682.9713	1.49	8	3	6	+	7	3	5	+	6682.9709	1.38
6683.0003	1.33	8	3	6	-	7	3	5	-	6683.0009	1.59
6683.4708	2.17	9	2	7	+	8	2	6	+	6683.4695	2.26
6683.4889	1.95	9	2	7	-	8	2	6	-	6683.4831	2.07
6683.5871	1.67	9	3	6	+	8	3	5	+	6683.5875	1.53
6683.6132	1.50	9	3	6	-	8	3	5	-	6683.6114	1.33
6683.7895	2.70	10	1	10	+	9	1	9	+	6683.7867	2.42
6683.7931	2.44	10	1	10	-	9	1	9	-	6683.795	2.00
6684.0502	2.34	10	2	9	+	9	2	8	+	6684.0501	2.40
6684.0643	2.12	10	2	9	-	9	2	8	-	6684.0622	2.54
6684.1998	1.65	10	3	8	-	9	3	7	-	6684.1988	1.51
6684.6337	2.48	11	2	9	+	10	2	8	+	6684.6299	2.40
6684.6399	2.26	11	2	9	-	10	2	8	-	6684.6405	2.21
6684.7677	1.78	11	3	8	-	10	3	7	-	6684.7617	1.74
6684.8441	2.97	12	1	12	+	11	1	11	+	6684.8417	2.73
6684.8475	2.73	12	1	12	-	11	1	11	-	6684.8516	2.99
6684.8698	1.41	11	4	7	+	10	4	6	+	6684.8664	1.57
6685.4378	1.39	12	4	9	-	11	4	8	-	6685.4353	1.42
6685.4994	3.17	13	0	13	+	12	0	12	+	6685.4968	3.00
6685.5011	2.94	13	0	13	-	12	0	12	-	6685.5014	3.32
6686.2844	2.17	14	3	12	+	13	3	11	+	6686.2842	2.66
6686.3000	2.02	14	3	12	-	13	3	11	-	6686.2990	2.17
6687.7459	1.66	17	4	13	+	16	4	12	+	6687.7460	1.92
6687.7651	1.57	17	4	13	-	16	4	12	-	6687.7644	1.38
6687.8327	2.73	18	2	17	+	17	2	16	+	6687.8305	2.87
6688.8602	1.50	20	4	17	-	19	4	16	-	6688.8599	1.37
6688.9925	2.00	21	3	18	+	20	3	17	+	6688.9907	2.01
6689.0364	2.70	23	0	23	+	22	0	22	+	6689.0330	3.27
6689.0388	2.58	23	0	23	-	22	0	22	-	6689.0465	2.38
6689.1672	1.45	21	4	17	-	20	4	16	-	6689.1750	1.22
6689.2739	1.92	22	3	20	+	21	3	19	+	6689.2702	1.69
6689.2782	1.83	22	3	20	-	21	3	19	-	6689.2820	1.84

The intensities are given in 10^{-24} $cm^{-1}/(molecule.cm^{-2})$ at 296K.
$ For the unresolved doublets, the total line intensity is given.

Figure(s)

Click here to download high resolution image

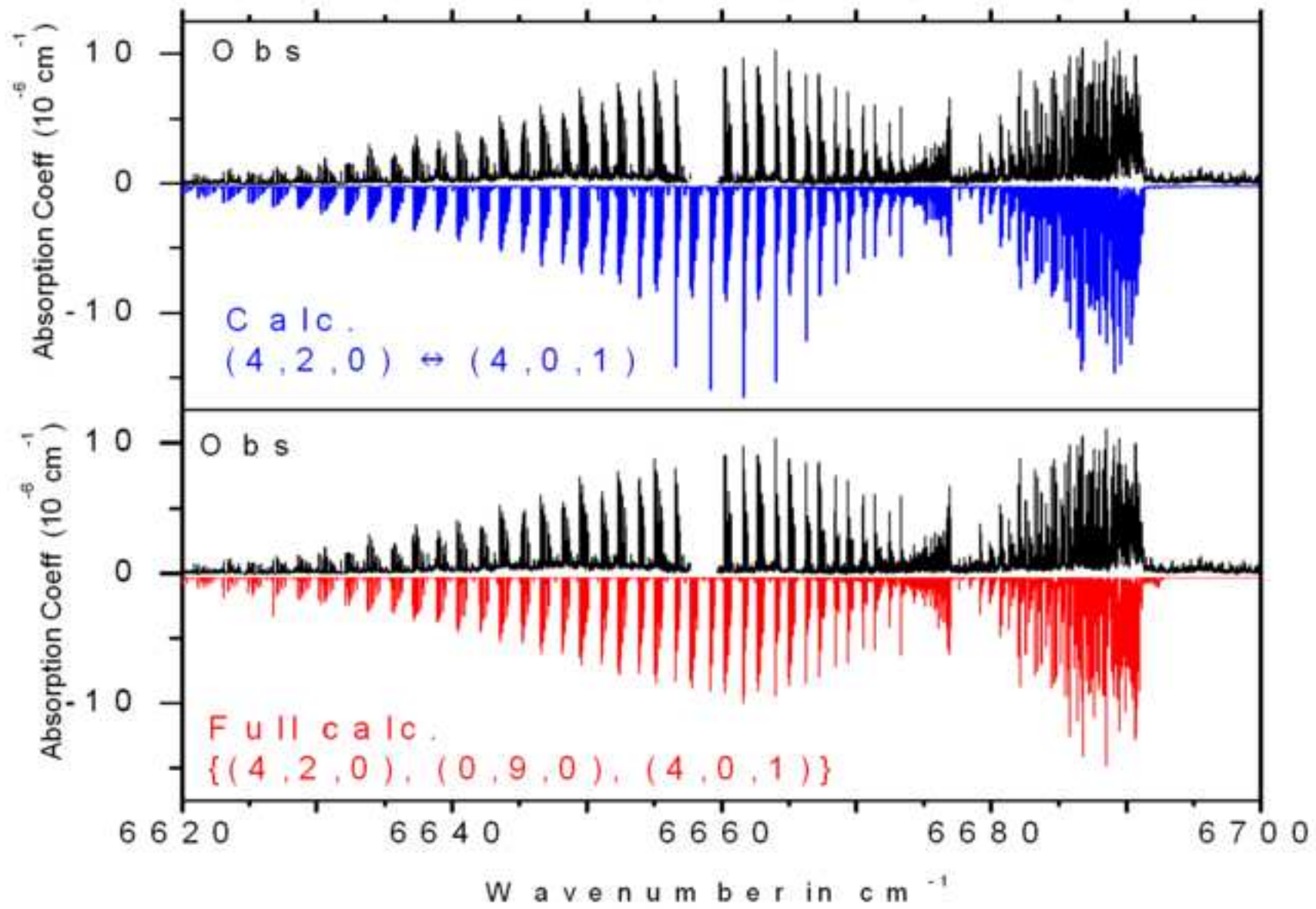

Fig.1

Figure(s)

Click here to download high resolution image

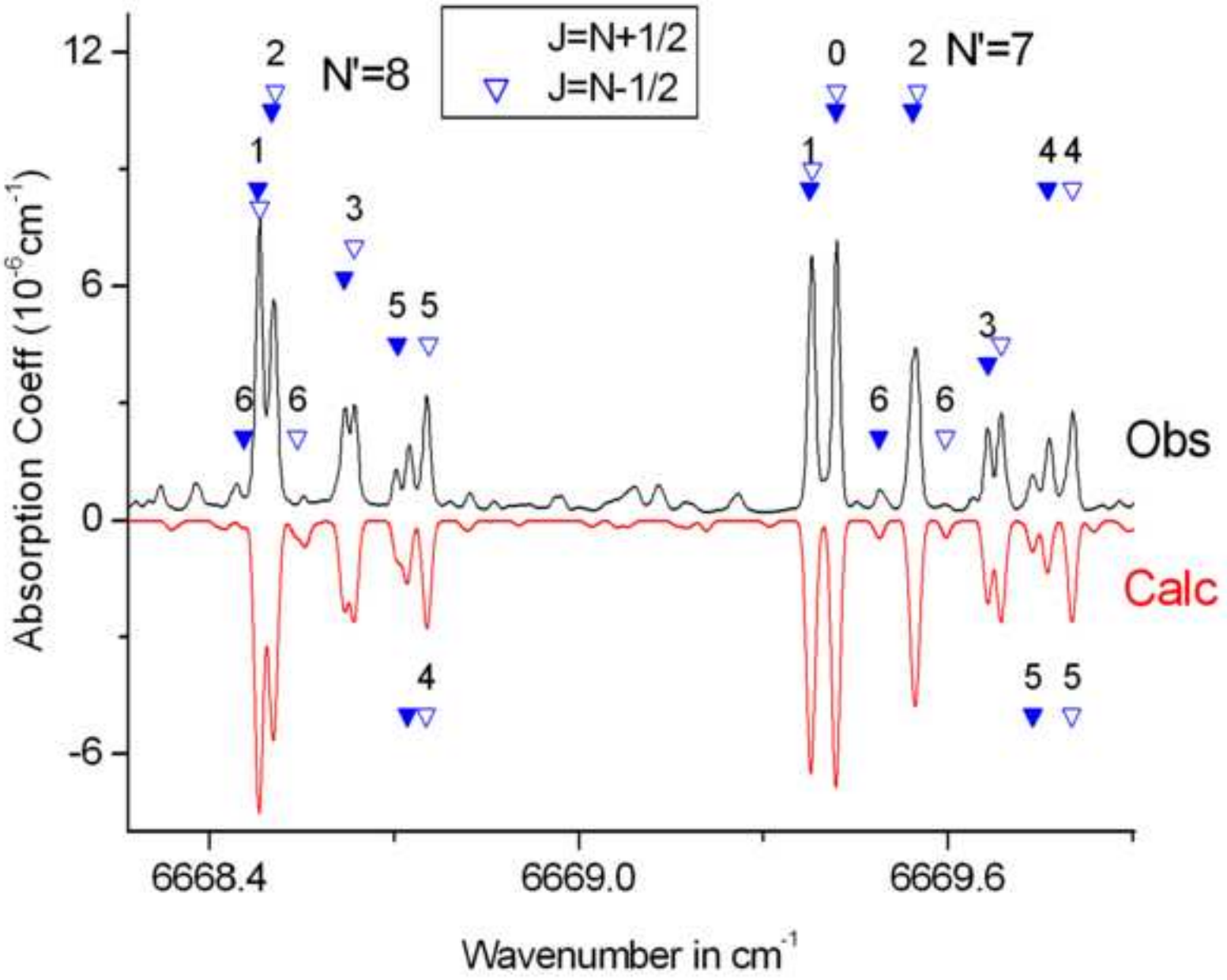

Figure(s)

Click here to download high resolution image

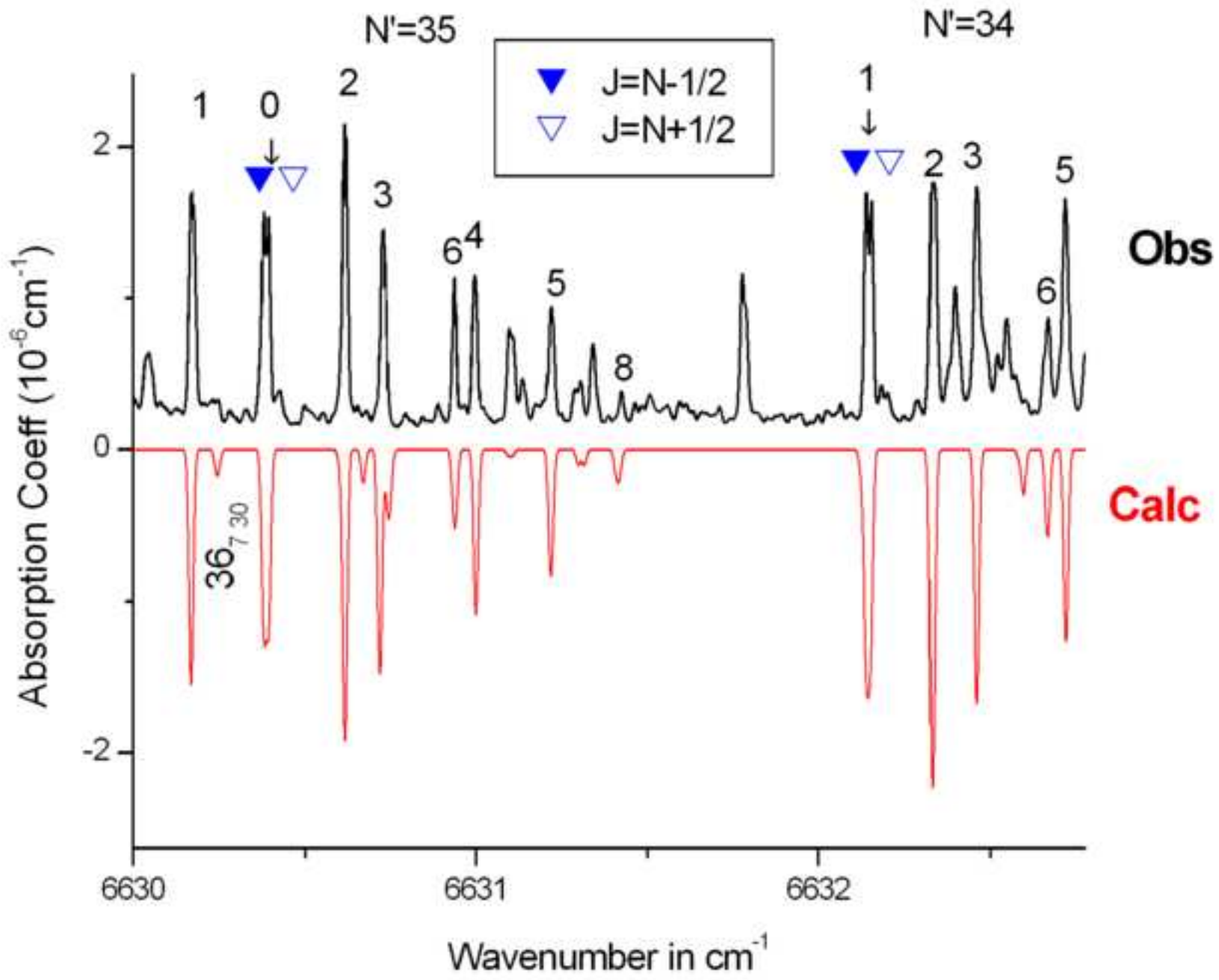

Figure(s)

Click here to download high resolution image

Fig.4

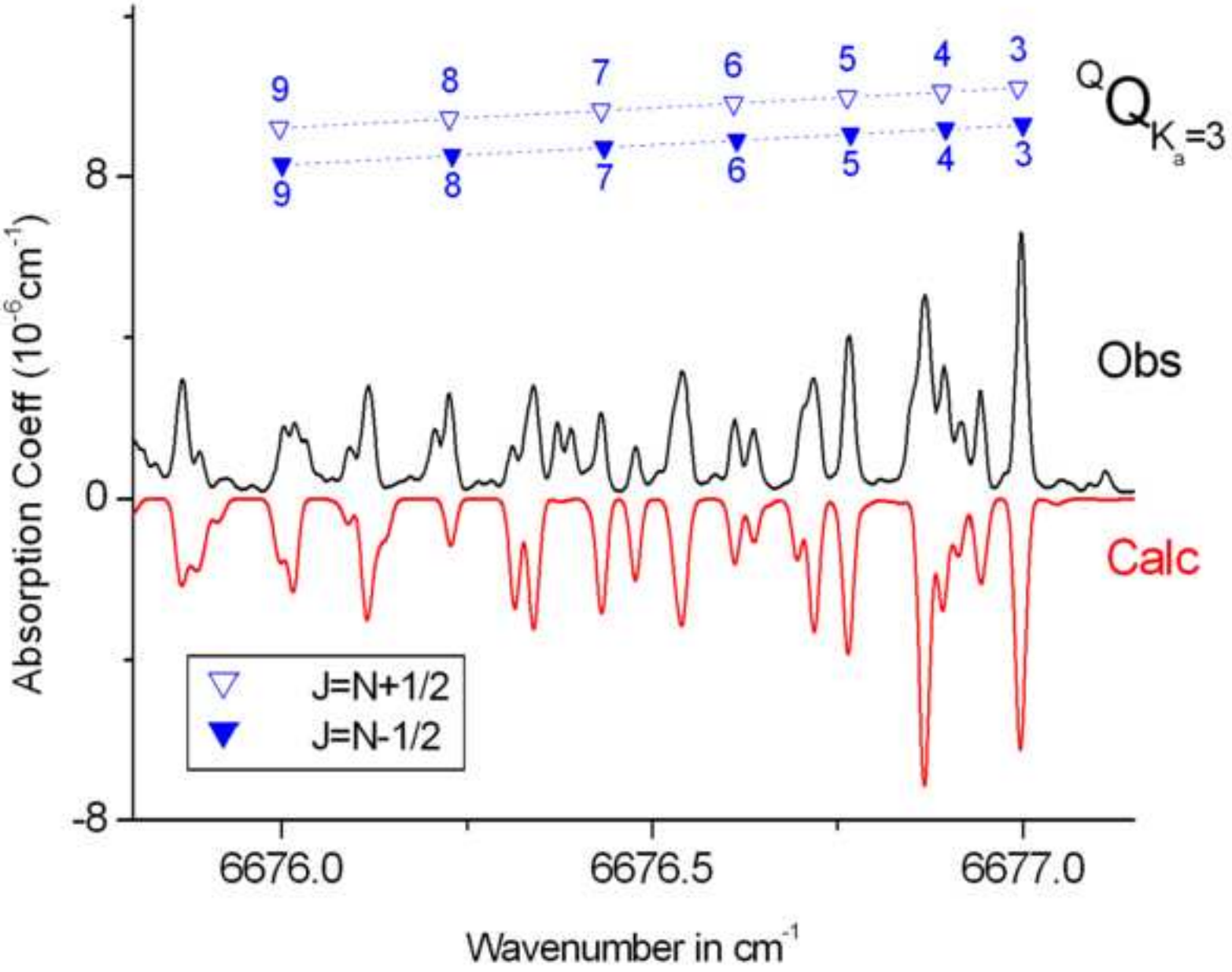

Figure(s)

Click here to download high resolution image

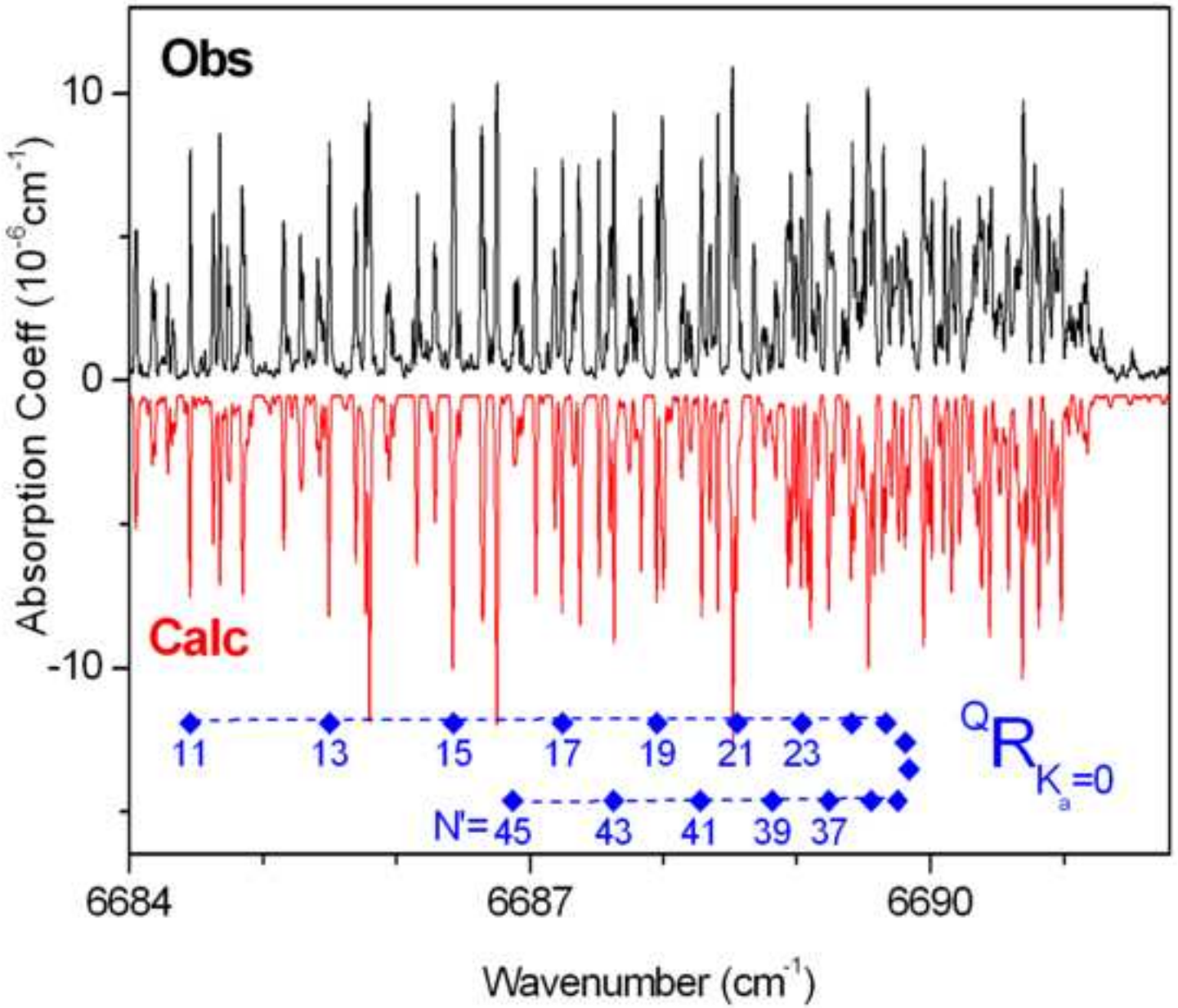

e-component, for online publication only

Click here to download e-component, for online publication only: Supplementary.TXT

e-component, for online publication only

Click here to download e-component, for online publication only: TFF401

e-component, for online publication only

Click here to download e-component, for online publication only: LL-NIVN